Materials Advances

PAPER

Check for updates

A ternary multiscale nanocomposite system based on functionalized graphene oxide, carbon fibers and bio-based polybenzoxazine for electromagnetic shielding

Madalina Ioana Necolau,[ab] Elena Iuliana Biru,[ab] Martino Aldrigo,[c] Elena Olaret,[a] Anamaria Zaharia,[d] Gabriela Ciuprina[e] and Horia Iovu [ID] *[ab]

Carbon fiber nanocomposites are widely used in numerous domains such automotive, aerospace, electronics and construction due to their excellent performance. They play a crucial role in electromagnetic shielding due to their unique electrical conductivity, lightweight structure, and mechanical strength. Over the last decade, the use of these materials has become more prominent and thus sustainability challenges related to both synthesis and processing should be considered while maintaining their properties in order to diminish their negative impact on the environment. Therefore, the present paper proposes a novel strategy to develop advanced nanocomposites based on bio-based benzoxazine, reduced graphene oxide functionalized with tetraethylene pentamine and carbon fibers (SP-GT-CF-PBz) with strong interfacial interactions between the components by harnessing the reactive nature of the bio-based benzoxazine monomer and graphene oxide brought by the free amino functionalities present on their structure and the $\pi-\pi$ interactions that may develop between benzoxazine, carbon fibers and graphene. The effects of GT loading over the curing behaviour of bio-based benzoxazine as well as its influence over the thermal and mechanical features of ternary nanocomposite systems containing carbon fibers have been systematically investigated. Differential scanning calorimetry (DSC) demonstrates that the addition of GT nanoflakes has a catalytic effect on the polymerization process, as a decrease in the maximum temperature of the exothermic peak as well as curing enthalpy was noted. The SP-GT2-CF-PBz nanocomposite laminate exhibits an enhanced nanomechanical modulus ($\sim$6 GPa) compared to SP-CF-PBz ($\sim$1 GPa) and good thermal properties. The present article provides a new insight into the investigation of compatibility and interaction between the bio-based benzoxazine monomer, graphene oxide and carbon fibers.

1. Introduction

The progressive evolution encountered in the nanotechnological field along with the continuous advancement of the industry has enforced the development of new advanced polymeric nanocomposites that will have the potential to significantly improve the quality of life.

[a] *Advanced Polymer Materials Group, National University of Science and Technology POLITEHNICA Bucharest, Romania. E-mail: horia.iovu@upb.ro*

[b] *Academy of Romanian Scientists, Ilfov 3, 050044 Bucharest, Romania*

[c] *National Institute for Research and Development in Microtechnology (IMT), Str. Erou Iancu Nicolae 126 A, 077190 Bucharest-Voluntari, Romania*

[d] *Advanced Polymer Materials and Polymer Recycling Group, National Institute for Research and Development in Chemistry and Petrochemistry-ICECHIM, Bucharest, Romania*

[e] *Faculty of Electrical Engineering, National University of Science and Technology Politehnica Bucharest, 313 Splaiul Independentei, 066042, Bucharest, Romania*

Bio-based benzoxazines have recently emerged as strong candidates for conventional petroleum-based thermosets due to their facile synthesis from natural compounds such as natural phenols (vanillin, sesamol, eugenol, guaiacol, lignin, and cardanol),[1–9] amines (furfurylamine and stearyl amine)[10,11] and aldehydes (salicylaldehyde).[12] These materials are characterized by superior mechanical properties and good thermal resistance owing to their aromatic nature conferred by the phenolic compound while exerting a strong resistance to chemicals.[13–15] The above-mentioned properties make benzoxazine resin a suitable candidate as a matrix for the design of green composite materials. Up to now, these thermosets have been successfully used alongside different nanostructures such as nano clays,[16,17] graphene oxide,[18–20] carbon nanotubes,[21] cellulose[22,23] and inorganic particles[24] to develop functional nanocomposites with improved thermal and mechanical features.

Most of the benzoxazine monomers used for composite preparation are in a solid state at room temperature and tend to polymerize at temperatures above 200 °C.[25] Thus, a viscous monomer with low curing temperature would significantly facilitate the processing of such materials subsequently reducing energetic consumption. Polyethyleneimine based benzoxazines[2,26,27] have recently emerged as viable bio-based monomers that not only lead to viscous and non-toxic monomers but also possess complex structures with multiple free amino groups. PEI's rich amine functionality facilitates ring-opening polymerization and may lead to highly crosslinked and thermally stable networks. Beyond sustainability, the PEI component also improves compatibility with nanofillers due to its ability to form strong interfacial interactions such as hydrogen bonds and possible covalent linkages with functionalized graphene oxide (GT) and carbon fibers.[28] This enhances filler dispersion and stress transfer within the composite. Compared to conventional resin systems such as epoxy, phenolic, or synthetic benzoxazines, the PEI-based bio-benzoxazine can provide a unique combination of tailored reactivity, structural tunability, and ecological advantage, making it a powerful matrix choice for high-performance nanocomposite applications. Additionally, it was already demonstrated that both primary and secondary amines have a significant influence on the curing process and can act as catalysts by reducing the ring-opening polymerization temperatures.[2,29,30] Zhang *et al.* used hexamethylenediamine as a curing agent for a commercially available benzoxazine monomer to synthesize foams through a sol–gel method at 30 °C.[31] Apart from the catalytic effect on the polymerization process, the amine curing of the benzoxazine resin improves the thermal and mechanical properties of the final network.[32]

As a particular class of engineered materials, nanocomposites benefit from state-of the art properties provided by both the organic matrix and the reinforcing agent required for industry, technology, and research fields. Carbon fiber-based nanocomposites are widely known for their incredibly lightweight, thermal and chemical resistance, superior mechanical properties and ease of fabrication.[33–35] Their use for example, in the aerospace and automotive industries and the medical field have motivated the researchers to boost their functionality towards the development of advanced systems. Over the last few years, carbon-based materials have become a valuable reinforcing agent for nanocomposites based on various polymers due to their valuable properties.[36–39]

Graphene oxide (GO) has emerged as a highly versatile nanomaterial in composite development due to its exceptional surface area, mechanical strength, and the abundance of oxygen-containing functional groups that enable strong interfacial interactions with polymer matrices. Its incorporation into various composites has been shown to significantly enhance mechanical, thermal, and electrical properties, making it a key component in the design of next-generation high-performance and multifunctional materials. Up to now, different GO derivatives bearing reactive functional groups such as carboxyl and amino have been successfully used in the development of advanced nanocomposite formulations.[40–43]

The continuous growth of technological fields along with the rapid evolution of electronic devices has led to an increase in electromagnetic pollution that can impact not only the environment but also human health. Protecting electronic devices from undesired interferences is of paramount importance in many telecommunication systems, especially in certain strategic frequency ranges, like the so-called X band spanning between 8.2 and 12.4 GHz. Most radars work in the X band, which is also allocated for terrestrial and space communications, as well as traffic light motion sensors and the radio frequency (RF) sources of particle accelerators. Electromagnetic interference (EMI) could be a dangerous source of serious problems through degradation of the performance of the affected electronics. To overcome this issue, during the last few years various lightweight materials have been investigated for EMI shielding purposes, such as conducting polymers, graphene, carbon nanotubes, and other nanocomposites.[44–46] In particular, the development of two-dimensional (2D) atomically thin materials has provided new solutions for EMI shielding with performance similar to those of carbon-based nanomaterials,[47–49] thus providing a major degree of freedom in materials science in tailoring the properties of new low-dimensional compounds in foams,[50] nanocomposites,[51] and liquid crystals[52] for EMI shielding.

In contrast to conventional composites that rely primarily on the reinforcing effect of carbon fibers or graphene-based fillers, the present study introduces a ternary nanocomposite system that emphasizes synergistic interactions between a bio-based benzoxazine matrix, reduced graphene oxide functionalized with tetraethylene pentamine (GT), and carbon fibers. The rich amine functionality of GT enables strong interfacial bonding with the reactive benzoxazine monomer, leading to enhanced dispersion and catalytic polymerization behavior.

The primary and secondary amine groups of tetraethylene pentamine (TEPA) have the potential to strongly interact with the oxazine rings, facilitating ring-opening polymerization and promoting strong interfacial adhesion. Additionally, TEPA can enhance the dispersion of GO in the polymer matrix by increasing its hydrophilicity and reducing aggregation tendencies. Compared to other functionalization agents, TEPA offers a unique combination of chemical reactivity and structural compatibility with the PEI-based benzoxazine matrix making it particularly effective in forming strong, thermally stable nanocomposites.[53,54]

The presence of both GT and carbon fibers can promote π–π stacking and hydrogen bonding within the matrix, resulting in a significant increase in tensile strength and thermal stability. Importantly, the use of a renewable benzoxazine monomer introduces a sustainable pathway for high-performance nanocomposites, distinguishing this work from traditional systems based on petroleum-derived resins and unmodified fillers.

The present study aims to develop a complex nanocomposite system with strong interfacial interactions between the components. Thanks to their mechanical and electrical properties, the synthesized ternary multiscale nanocomposite systems integrating functionalized reduced graphene oxide, carbon

fibers, and bio-based polybenzoxazine can be profitably used in electromagnetic interference (EMI) shielding applications.

2. Experimental

2.1. Materials

Bio-based benzoxazine based on sesamol and polyethylene-imine previously synthesized and characterized by our team was used as a polymeric matrix (SP-Bz).[27] Reduced graphene oxide tetraethylene pentamine functionalized (GT) from NanoInnova Technologies (Spain) (containing 1.1 mmol NH_2/g) and commercially available 3 K, 2×2 Twill Weave Carbon Fiber Fabric (CF) from FibreGlast were used as received.

2.2. Nanoreinforced prepreg synthesis

Different concentrations of GT (1%, 2% and 3% wt, respectively were selected based on literature precedents and practical considerations[55–57]) were dispersed by ultrasonication within the SP-Bz monomer for 30 minutes over an ice bath in order to prevent local heating and degradation of both polymeric matrix or graphene flakes. Collado et al.[57] have demonstrated in their study that the physical properties and performance of the final material are altered by increasing ultrasonication time when dispersing graphene oxide into epoxy resin through ultrasonication for more than 30 minutes.

The resulting nanoreinforced resins (SP-GT-Bz) were then dispersed between two carbon fabric layers. The impregnation was then facilitated with the help of a mechanical press where a small pressure was applied. Further on, the obtained prepregs were degassed at 80 °C for 15 min followed by thermal polymerization as follows: 1 h-100 °C, 1 h-120 °C, 1 h-140 °C, 1 h-160 °C and 1 h-180 °C.

A schematic representation of the synthesis process is represented in Fig. 1. The composition and abbreviations of all samples are presented in Table 1.

Table 1 Nanocomposite material composition and abbreviations

Sample	Monomer	GT	CF	Abbreviation	Abbreviation for the cured nanocomposites
1.	SP-Bz	—	—	SP-Bz	SP-PBz
2.	SP-Bz	1%	—	SP-GT1-Bz	SP-GT1-PBz
3.	SP-Bz	2%	—	SP-GT2-Bz	SP-GT2-PBz
4.	SP-Bz	3%	—	SP-GT3-Bz	SP-GT3-PBz
5.	SP-Bz	—	CF	SP-CF-Bz	SP-CF-PBz
6.	SP-Bz	1%	CF	SP-GT1-CF-Bz	SP-GT1-CF-PBz
7.	SP-Bz	2%	CF	SP-GT2-CF-Bz	SP-GT2-CF-PBz
8.	SP-Bz	3%	CF	SP-GT3-CF-Bz	SP-GT3-CF-PBz

2.3. Equipment and characterization

X-ray photoelectron spectrometry (XPS) analysis was performed on a K-Alpha spectrometer with a monochromatic Al Kα source (1486.6 eV) working under a vacuum base pressure of 2×10^{-9} mbar. Charging effects were compensated using a flood gun, and binding energy was calibrated by placing the C 1s peak at 284.8 eV as an internal standard. Deconvolution of C 1s peaks was performed by using a smart background algorithm with a convoluted Gaussian–Lorentzian ratio. The pass energy for the survey spectra was set at 200 eV, and it was 20 eV for the high-resolution spectral registration.

Differential scanning calorimetry (DSC) analyses were conducted on a Netzsch DSC 204 F1 Phoenix instrument under a nitrogen atmosphere (20 mL min^{-1} flow rate) from 20 to 300 °C. The curing properties were assessed by employing heating rates of 5, 10, 15, and 20 °C min^{-1}. Kinetic parameters of nanoreinforced benzoxazine systems were evaluated through non-isothermal DSC analysis. The apparent activation energy (E_a) was computed with the aid of modified Kissinger (1) and Ozawa (2) equations:[58]

$$\ln\left(\frac{\beta}{T_P^2}\right) = \ln\frac{AR}{E_a} - \frac{E_a}{RT_p} \tag{1}$$

$$\ln \beta = -1.05 E_a R T_p + C \tag{2}$$
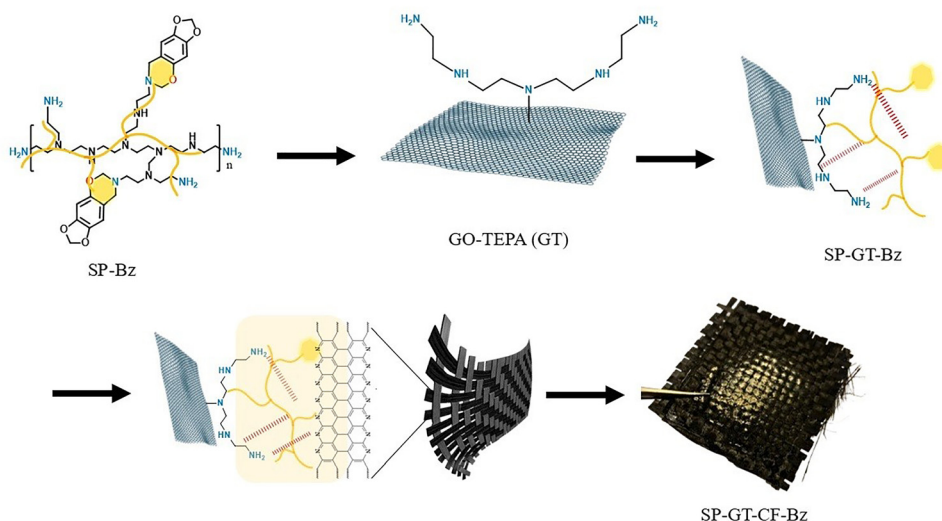

SP-Bz

GO-TEPA (GT)

SP-GT-Bz

SP-GT-CF-Bz

Fig. 1 Schematic representations of the main steps involved in the development of SP-Bz nanoreinforced prepregs.

where E_a is the activation energy (kJ mol^{-1}), β is the heating rate (°C min^{-1}); T_p is the maximum temperature of the polymerization peak (K); A is the pre-exponential factor; R is the gas constant ($R = 8.314$ J mol^{-1} K^{-1}) and C is a constant.

Additionally, E_a values were calculated using the model-free Ozawa–Flynn–Wall (OFW) isoconversional method, based on the temperature dependence of conversion rates at different heating rates.

Dynamic-mechanical analysis (DMA) tests were performed using a TRITEC 2000 B instrument in single cantilever bending mode at 1 Hz frequency in the temperature range of 25 to 240 °C with a heating rate of 5 °C min^{-1}. Crosslinking density (ρ_x) was calculated for the cured networks based on DMA results, considering that the crosslinking density of polymers can be quantitatively determined from the equilibrium storage modulus in the rubbery region using the following equation:[59]

$$\log\left(\frac{E'_e}{3}\right) = 7 + 293(\rho_x) \tag{3}$$

Crosslinking density values were calculated from the storage modulus in the rubbery region (T_g + 30 °C) using the classical rubber elasticity equation. This common approach assumes ideal network behaviour, which may not fully represent rigid or phase-separated systems; thus, the results are considered relative indicators for comparing sample networks rather than absolute values.

The efficiency of various fillers in composite materials can be represented by the coefficient of "C" that can also be calculated based on DMA results with the aid of the following equation:[60]

$$C = \frac{\left(\dfrac{E'_g}{E'_r}\right)\text{composite}}{\left(\dfrac{E'_g}{E'_r}\right)\text{matrix}} \tag{4}$$

where E'_g represents the value of the storage modulus in the glassy state and E'_r is the value of the modulus in the rubbery state.

Thermogravimetric analyses (TGA) were done using a TG 209 F1 Libra instrument analyzer. Approximately 10 mg from each sample were subjected to heating in the temperature range 20–700 °C with a heating rate of 10 °C min^{-1} under a nitrogen atmosphere. The residual mass after thermal analysis was later used to determine the limiting oxygen index (LOI) with the aid of the following equation:[61]

$$\text{LOI} = 17.5 + 0.4 \times \text{residual mass} \tag{5}$$

Contact angle measurements (CA) were performed on a DSA100E (KRUSS GMBH) equipment under static conditions by employing the Sessile drop method using water and ethylene glycol as probing liquids. The reported results comprise the average of three measurements by using Young–Laplace fitting.

The water absorption degree (WA%) was measured for the synthesized ternary nanocomposites following the EN 2378 standard.[62,63] For this, three specimens from each sample were precisely weighed (m_0) and then placed in distilled water at 25 °C and 80 °C where they were kept for 14 days. After 1, 3, 7 and 14 days, the specimen was extracted, the excess solvent was removed with filter paper and the final weights were recorded (m_x). The WA% values were calculated with the aid of the following equation:

$$\text{WA\%} = \frac{m_x - m_0}{m_0} \times 100 \tag{6}$$

A scanning electron microscope (SEM) (HitachiTM4000plus II tabletop, Spectral, Lidingo, Sweden) with a cooling stage and 15 kV operation was used to examine the morphological features of all the samples that were analyzed. A thin layer of electrically conductive gold was applied to the samples prior to analysis in order to prevent "charging", in this way diminishing thermal damage and increasing secondary electron emission.

Local mechanical properties were determined through nanoindentation tests using a G200 Nanoindenter (KLA Instruments, USA). A Berkovich diamond tip with a radius of 20 nm was used to perform each indentation while assuring at least 50 µm distance between them. The displacement was set to 2000 nm and the modulus (E) and hardness (H) were measured using a continuous stiffness measurement (CSM) method.

Statistical analysis. All experiments were performed in triplicate ($n = 3$) and the results for the quantitative assays were expressed as a mean ± standard deviation (SD) using GraphPad Prism Software 8.0 (GraphPad Software Inc., San Diego, CA, USA). Statistical relevance was assessed using the same software, a one-way ANOVA method and post-test Bonferroni considering significant statistical differences for $p < 0.05$.

Electromagnetic (EM) shielding properties of the nanocomposite samples were assessed by employing a calibrated vector network analyzer (VNA) connected to two X-band waveguide transitions, and in between the latter, we inserted the various specimens to register the S parameters at the two ports of the VNA as previously described in our work.[50–52] Thus, their reflection and transmission properties were determined in a particular frequency range from 8.2 to 12.4 GHz, known as the X band.

The shielding properties of the materials under test (MUTs) were evaluated by calculating the total EM shielding effectiveness (SE), which is given by the following formula:

$$\text{SE(dB)} = \text{SE}_R(\text{dB}) + \text{SE}_A(\text{dB}) \tag{7}$$

where SE_R is the shielding effectiveness related to EM reflections (R) and SE_A is the shielding effectiveness related to absorption (A) phenomena. SE_R and SE_A can be calculated using the measured scattering (S) parameters in the X band, i.e., the reflection (S_{11} or S_{22}) and transmission (S_{21} or S_{12}) parameters:

$$\begin{aligned}\text{SE(dB)} &= \text{SE}_R(\text{dB}) + \text{SE}_A(\text{dB}) \\ &= 10\log\left[\left(1 - |S_{11}|^2\right)^{-1}\right] + 10\log\left[\frac{(1 - |S_{11}|^2)}{|S_{21}|^2}\right]\end{aligned} \tag{8}$$

The two main physical mechanisms to modulate SE are EM reflections (strongly increased in the case of metals and absorption due to dielectric losses and low conductivity).

We stress here that the measurement setup does not allow the mechanical flexing of the samples, as they need to cover the whole aperture of the X-band waveguides. For the same reasons, experiments with different thermal cycling conditions are difficult to perform.

3. Results and discussion

3.1. Structural characterization of GT and CF through elemental analysis

The surface composition of GT and CF was analyzed by XPS in order to identify the main atoms that may further generate interactions with the components of the nanocomposite system. The XPS survey and high-resolution C 1s of GT and CF are shown in Fig. 2.

The surface of GT consists mainly of carbon (284.69 eV, 80.98%), oxygen (530.96 eV, 9.76%), and nitrogen (398.36 eV, 9.27%) elements. The same elements were also detected in the case of the CF sample in different concentrations. The presence of oxygen and nitrogen on both reinforcing agents demonstrates the existence of possible active sites for additional interactions within the nanocomposite formulations.

3.2. Differential scanning calorimetry (DSC)

Prior to composite preparation, the curing behavior and the influence of the nanoreinforcing agent over the benzoxazine polymerization process were assessed by employing differential
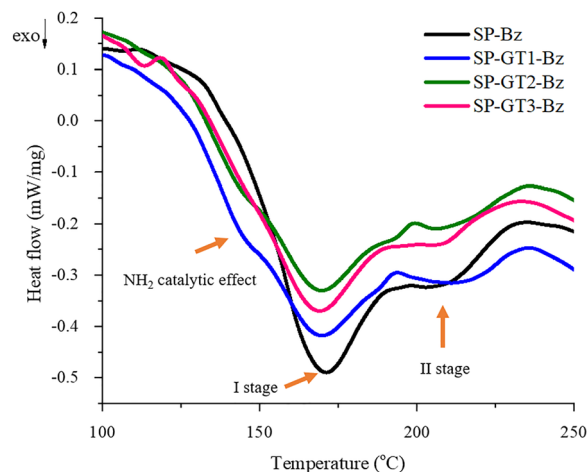

Fig. 3 Curing profiles of SP-BZ and its GT nano-reinforced systems.

scanning calorimetry. The DSC thermograms are displayed in Fig. 3 and the corresponding parameters are presented in Table 2.

When analyzing the curing profile of both monomer and nanocomposite systems, one can observe the presence of a broad signal with a shoulder shifting to higher temperatures. This complex exothermal event may be a consequence of the intricate structure of the SP-Bz monomer suggesting that the curing reaction relies on two distinct mechanisms that occur at different stages.[64,65] We can assume that in the first stage of the
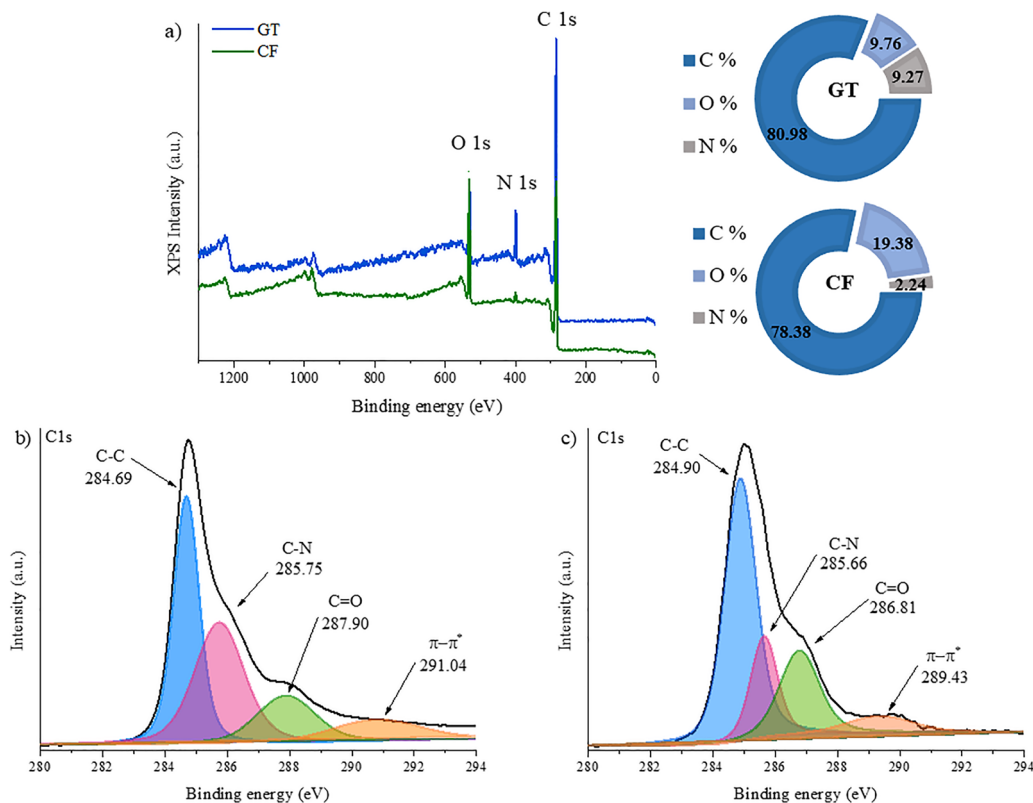

Fig. 2 Survey and elemental composition of GT and CF (a), C 1s of GT (b), and C 1s of CF (c).

Table 2 DSC data of SP-BZ and its nano reinforced systems

Sample	ΔH_1 (J g^{-1})	T_{max1} (°C)	T_{max2} (°C)
SP-Bz	128.6	171.2	208.1
SP-GT1-Bz	110.5	169.8	213.7
SP-GT2-Bz	101.6	169.8	210.8
SP-GT3-Bz	97.59	169.1	207.6

curing process the polymerization of benzoxazine moieties takes place while in the second stage additional interactions occur between the multiple free amino groups present on the backbone of the monomer. By analyzing the allure of the peaks describing the curing process, it can be observed that in the case of the first stage, the symmetrical signal may suggest that the autocatalytic nature of benzoxazine ring opening process lead to homogeneous species within the system while the broader second event may indicate some secondary interactions within the network promoted by higher temperature.[66] In the case of the samples containing GT, a small shoulder appears on the thermogram around 140 °C sustaining the catalytic effect of the carbon-based nanostructure over the reaction kinetics.[67]

As can be seen from the data shown in Table 2, the introduction of GT shifts the exothermic peak of the polymerization process towards lower temperatures. The T_{max1} values, which range from 169.1 °C to 171.2 °C for all samples, are rather close, suggesting that the dispersion of GT layers exhibits no significant effect on the first step of the curing process. However, the decrease in polymerization temperature as a function of GT concentration used in each case may be generated by the additional functionalities present on the surface of the carbonaceous nanostructure. In contrast with the trend followed by T_{max1}, the maximum of the second thermal event (T_{max2}) has the highest value for the SP-GT1-Bz (~214 °C) while SP-GT3-Bz has the lowest T_{max2} (207.6 °C). Despite the low concentration of GT (1%), due to network formation in the first stage of the curing process, the reactive amino groups are hindered by the chains formed within the network and thus the catalytic effect exerted by these functionalities is diminished. A similar catalytic effect over the benzoxazine curing process was observed by Garcia-Martinez at 2% graphene oxide concentration due to functional groups present on its surface.[68]

In comparison to the other samples, the SP-Bz had the largest ΔH_1 (128.6 J g^{-1}), indicating a more exothermic curing response. The addition of GT layers could lower the total energy released during the curing process, as evidenced by the decreasing enthalpy values as the concentration of GT enhances from

GT1 to GT3. This may imply that the presence of GT modifies the system's reactivity. This may demonstrate that the amino groups present on the surface of graphene oxide act as incentive catalysts for the oxazine ring opening process (C–O cleavage).

For a better understanding of the influence of the GT over the curing process of the SP-Bz monomer, the apparent activation energy (E_a) was computed by employing modified Kissinger and Ozawa methods. Both techniques provide a significant advantage for the studied system due to the fact that they allow the calculation of the kinetic parameters without prior insights into the reaction mechanism. The kinetic data presented in Table 3 display a complex curing mechanism that according to the two dominant exothermal events present on the thermogram (Fig. 3) takes place in two main steps. In the case of the first stage of the curing process, the activation energy of SP-Bz monomer is in a range similar to other data reported in the literature corresponding to an autocatalytic mechanism.[68] SP-Bz has the highest activation energy values in stage I, with 112.8 J mol^{-1} (Kissinger) and 114.4 J mol^{-1} (Ozawa). This suggests that the curing reaction for the PBz is relatively more energy-intensive in the initial stage, indicating a slower polymerization reaction.

The activation energy values for the GT-filled materials in the second stage are significantly higher than in the first stage, indicating a shift in the reaction mechanism. SP-GT1-Bz shows a dramatic increase to 327.5 J mol^{-1} (Kissinger) and 319.1 J mol^{-1} (Ozawa), which suggests that the presence of GT may lead to a more diffusion-controlled process in the second stage, where the mobility of reactive species is limited. Similarly, SP-GT2-Bz and SP-GT3-Bz also exhibit high activation energy values in stage II (239.7 J mol^{-1} and 280.4 J mol^{-1}, respectively), indicating that the curing process becomes more difficult to control as the reaction progresses (Fig. 4).

The evolution of activation energy (E_a) as a function of conversion (α) was evaluated using the Ozawa–Flynn–Wall (OFW) isoconversional method based on non-isothermal DSC data. This approach was applied to the neat benzoxazine resin (SP-Bz) and to three composite systems incorporating GT (SP-GT1-Bz, SP-GT2-Bz, and SP-GT3-Bz) and the corresponding results are presented in Fig. 5.

The neat benzoxazine sample (SP-Bz) exhibited a gradual increase in E_a across the conversion range, starting from ~90 kJ mol^{-1} and rising progressively toward higher values at $\alpha > 0.8$, reaching values above 140 kJ mol^{-1} near complete curing. This trend reflects the multi-step nature of benzoxazine polymerization, involving initial ring-opening of the benzoxazine

Table 3 Kinetic parameters of the curing reactions of SP-BZ and its GT based nanocomposites

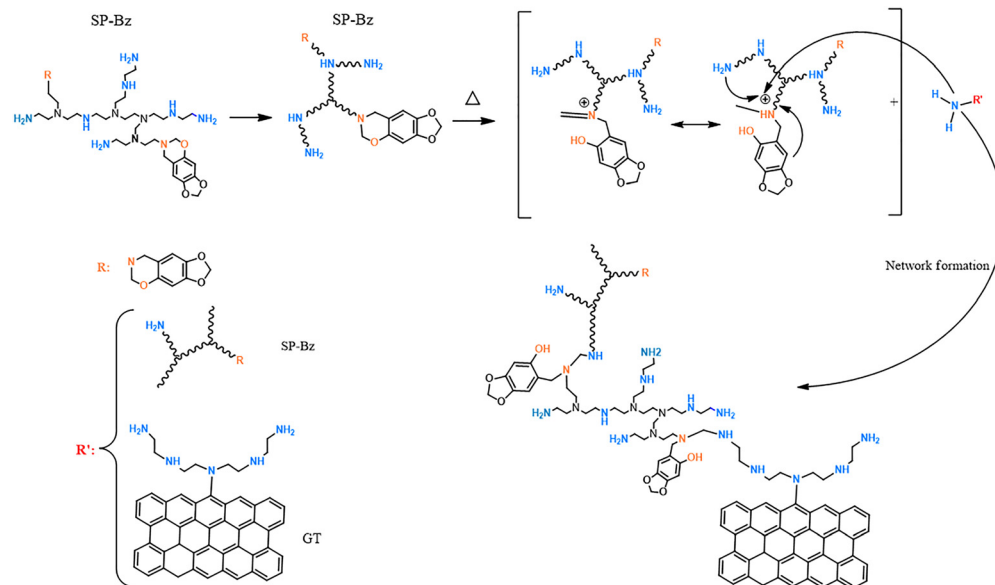| Sample	Stage I		Stage II	
	Activation energy Kissinger	Activation energy Ozawa	Activation energy Kissinger	Activation energy Ozawa
SP-Bz	112.8	114.4	122.5	124.1
SP-GT1-Bz	98.1	100.4	327.5	319.1
SP-GT2-Bz	83.7	86.7	239.7	235.4
SP-GT3-Bz	88.3	91.1	280.4	274.3

Fig. 4 Proposed reaction mechanism for the amine catalyzed benzoxazine ring opening reaction.
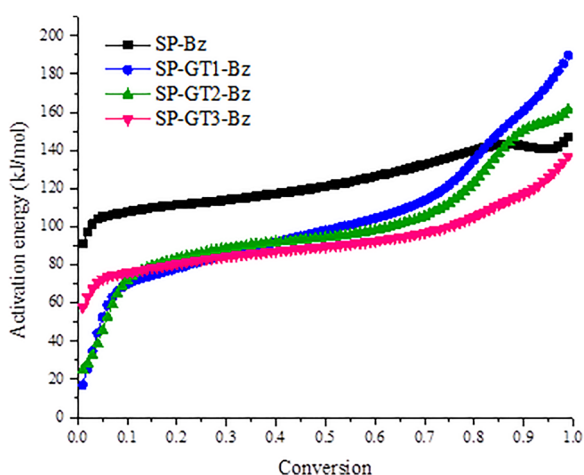

Fig. 5 The evolution of activation energy (E_a) as a function of conversion (α).

conversion range. Analysing the SP-GT3-Bz sample, one can observe that it presents the lowest E_a at low conversion ($\sim$60 kJ mol^{-1}), further confirming the catalytic role of GT. However, at higher conversions, the energy requirement increases gradually. This may be attributed to nanofiller agglomeration or reduced segmental mobility, which hinder the final stages of crosslinking. Thus, SP-GT2-Bz sample emerges as the most kinetically favorable, maintaining low to moderate E_a values throughout the curing process.

This isoconversional analysis is consistent with the Kissinger- and Ozawa-derived average activation energies listed in Table 3, further supporting the validity of our findings. Moreover, it provides additional mechanistic insight into how TEPA-functionalized graphene oxide influences the reaction pathways at different stages of curing.

moiety, propagation, cross-linking, and vitrification. The gradual increase in E_a is consistent with diffusion-controlled kinetics and increasing network rigidity at higher conversions.[66,69]

In contrast, all GT-functionalized systems demonstrate significantly reduced activation energies at low conversion, sustaining the catalytic effects attributed to the amine functionalities of GT. The extent and nature of this catalytic influence vary with GT content. The lowest value for E_a was determined for the SP-GT1-Bz sample ($\sim$20 kJ mol^{-1}), suggesting effective catalytic initiation. However, a steep increase is observed at $\alpha > 0.7$, possibly due to mobility restrictions or filler–matrix interactions that hinder chain rearrangement and crosslinking. SP-GT2-Bz displays a relatively smooth and moderate evolution of E_a along with conversion. This reflects a favourable balance between catalytic activity of the amine species over the curing reaction and minimal diffusional hindrance, resulting in efficient crosslinking throughout the

3.3. Thermal properties

The thermal stability of SP-GT-PBz and SP-GT-CF-PBz nano-composites was evaluated through thermogravimetric analysis and the corresponding thermograms are presented in Fig. 6. The data corresponding to the most significant stages of the degradation process are shown in Table 4.

SP-PBz shows good thermal resistance at a $T_{d5\%}$ of around 238 °C. Along with the incorporation of GT there is a slight decrease in the case of the 1% composite, probably due to the degradation of the additional functionalities present on the surface of the graphene sheets. However, optimal thermal resistance is achieved in the case of the SP-GT2-PBz sample sustaining that this is the ideal composition to strengthen the overall properties of the system.

In the case of the ternary nanocomposite systems, the over-all thermal properties are improved. This may be caused by the binding of GT with the benzoxazine matrix through H-bonding
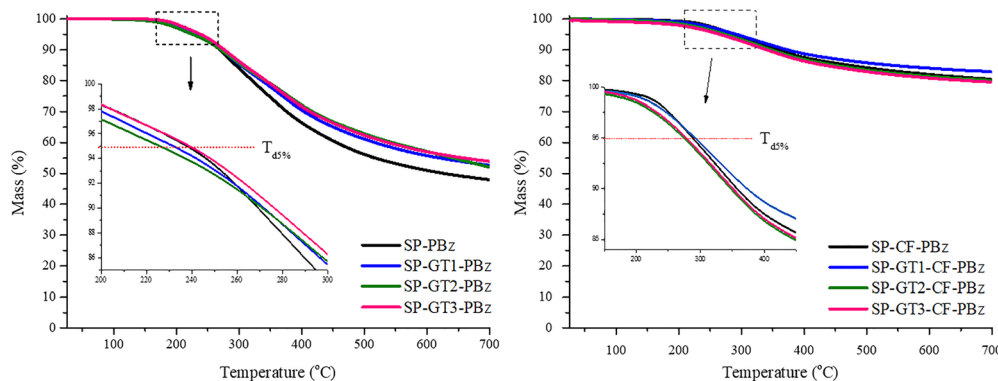
Fig. 6 TGA degradation profiles for bio-benzoxazine nanocomposite samples in a nitrogen atmosphere.

Table 4 TGA data recorded for bio-based nanocomposites under a N$_2$ atmosphere

Sample	$T_{d5\%}$ (°C)	$T_{d10\%}$ (°C)	Residual mass (%)	T_{max} (°C)		LOI (%)
GT	196.9	295.5	71.4	339.7		—
CF	407.1	666.2	88.1	—		—
SP-PBz	238	269	48	278	368	36.7
SP-GT1-PBz	231	272	53	285	367	38.7
SP-GT2-PBz	256	271	52	290	377	38.3
SP-GT3-PBz	239	276	48	288	367	36.7
SP-CF-PBz	288	357	81	333		49.9
SP-GT1-CF-PBz	292	373	83	316		50.7
SP-GT2-CF-PBz	274	348	80	317		49.5
SP-GT3-CF-PBz	272	334	77	335		48.3

and by the strong π–π interactions exerted between the carbon-based structures.

The residual mass (%) after thermal degradation is an important indicator of char formation and thermal stability. SP-PBz has a residual mass of 48%, while SP-GT1-PBz shows a slight increase to 53%. This suggests that the addition of GT contributes to char formation, enhancing thermal stability. SP-CF-PBz exhibits a significantly higher residual mass of 81%, indicating that CF reinforcement greatly improves the thermal stability and char yield of the nanocomposite, probably due to its high thermal resistance.

Residual mass is an important parameter that can be used to calculate the limiting oxygen index (LOI) that provides valuable information related to thermal resistance of polymeric materials. Generally, materials with LOI values above 28% can be considered as self-extinguishing.[70]

SP-PBz has a LOI of 36.7%, indicating moderate flame resistance. The LOI increases with the addition of graphene, with SP-GT1-PBz achieving a LOI of 38.7%, suggesting improved flame retardancy. As expected, along with the incorporation of CF within the system SP-CF-PBz shows the highest LOI at 49.9%, indicating excellent flame resistance, which is expected due to the high thermal stability and char formation associated with carbon fiber. This may also be attributed to synergistic interactions among the bio-based benzoxazine matrix, GT, and carbon fibers. The ternary system promotes the formation of a continuous, thermally stable char layer during combustion, which serves as a protective barrier against

heat and oxygen penetration.[71,72] The amine functionalities on GT enhance crosslinking and restrict polymer degradation pathways, further increasing char yield.[56,73] Additionally, the well-dispersed, high aspect ratio fillers create tortuous paths that delay volatile release and oxygen diffusion.[55]

The varying effects of different graphene oxide/CF concentrations suggest that there is an optimal loading level that maximizes thermal properties, as seen with SP-GT1-CF-PBz. We can assume that in this case the interlocking action of GO between the benzoxazine matrix and CF lead to a more stable network.

The DTG curves for SP-PBz and its corresponding graphene composites (Fig. 7) display a classical degradation profile for benzoxazine resins, where the initial decomposition of nitrogen-containing functionalities occurs around 300 °C, while at higher temperatures (above 400 °C) the cleavage of the Mannich base takes place.[74,75] An additional degradation transition occurs for the nanocomposites around 200 °C that may be associated with the moisture evaporation[76] or thermal decomposition of residual functional groups such as (epoxide, COOH) that may exist on the basal plane of the reduced graphene oxide.[77]

3.4. Thermomechanical properties (DMA)

The reinforcing effect of GT over the storage modulus of bio-based CF nanocomposites was evaluated through dynamic mechanical analysis and the corresponding thermograms are presented in Fig. 8.

Up to now, bio-based benzoxazine demonstrated strong potential for further use as substitutes for conventional petroleum-based thermosets. However, most of the studied bio-based resins possessed weak mechanical properties. In order to overcome this limitation along with the inherent brittleness, CF reinforcement came as a viable solution due to their widely known superior mechanical resistance.[78–81] The storage modulus for SP-CF-PBz increases by 340-fold as compared with the neat polybenzoxazine system and continues to increase with the addition of GT over the whole temperature range. The improvement of the mechanical properties exerted by the amino enriched graphene nanoflakes may be due to a synergistic effect between the numerous amine functionalities that subsequently lead to a secondary hydrogen bond network.
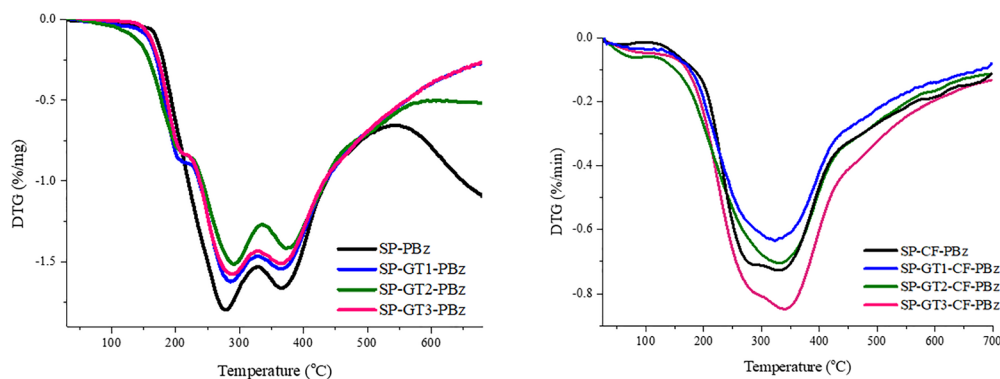
Fig. 7 DTG degradation profiles for bio-benzoxazine nanocomposite samples in a nitrogen atmosphere.
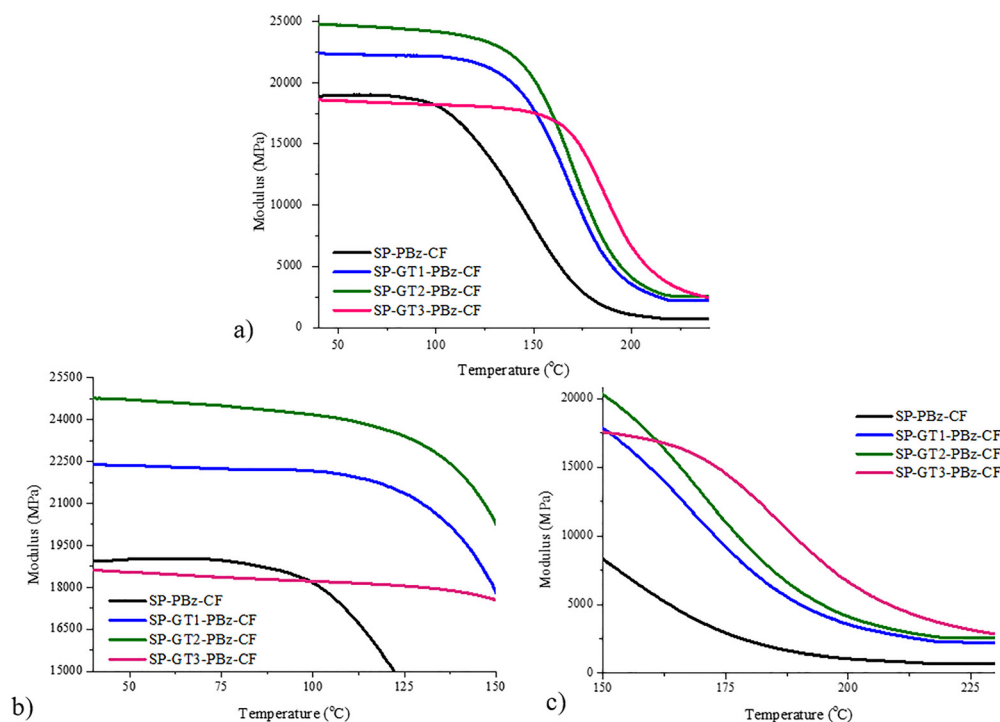

Fig. 8 The reinforcing effect of GT on storage modulus for CF bio-based nanocomposites (a), storage modulus in the glassy state (b) and in the rubbery state (c).

The modulus in the glassy state is mainly driven by the arrangement of the polymeric chains within the network and the intermolecular interactions and forces.[82] The storage modulus values of GT reinforced SP-Bz composites reached the maximum value when graphene mass concentration was 2 wt% due to the homogeneous dispersion of the nanofiller within the polymer matrix. This may suggest that at this concentration a percolation threshold effect occurs, suggesting that this is the maximum concentration at which the nanofiller potentiates the mechanical performance of the system. Beyond 2% concentration, the benefits may be not significant or diminish due to GT agglomeration, which can negatively impact the nanocomposite performance. Despite the highest value for the T_g of 3% GT nanocomposite sample, the modulus value is lowered. In this case, the increased concentration may lead to agglomeration of

the carbonaceous nanoflakes, thus creating points of tension within the material.

While the concept of percolation threshold is well-established in the context of electrical conductivity and the formation of continuous conductive networks in polymer composites,[83–85] its direct correlation with mechanical performance is less straightforward. In this study, changes in dynamic mechanical analysis (DMA) data with increasing filler content were observed, indicating modifications in the network structure and stiffness. However, we recognize that DMA alone cannot reliably determine the electrical or mechanical percolation threshold. Therefore, the term "percolation threshold" is used here qualitatively to describe the transition region where filler–filler interactions begin to significantly influence composite properties, rather than a strict, quantitatively defined

threshold. This interpretation aligns with previous reports where mechanical percolation has been discussed in relation to filler content and property changes.[85,86]

T_g increases with the addition of graphene and carbon fiber, with SP-GT3-CF-PBz reaching the highest T_g of 208 °C. The nanofillers significantly enhance the mechanical properties of the polymer matrix, more likely due to improved interactions between the GT/CF and the PBZ chains, which restrict molecular mobility.[59]

Although an increase in T_g was observed at 3 wt% GT loading, the corresponding decrease in the storage modulus suggests a decoupling effect between thermal and mechanical behaviour. This apparent contradiction can be attributed to several factors. At higher GT concentrations, the likelihood of nanofiller agglomeration increases, which can compromise the integrity of the interfacial region and reduce the efficiency of stress transfer within the composite. Additionally, the high density of amine functionalities on TEPA-functionalized rGO may introduce localized flexibility at the polymer–nanofiller interface, acting as a plasticizing domain that diminishes stiffness. Despite this, the restricted segmental mobility of the polymer chains near the rigid GT nanoflakes may still elevate T_g, as molecular motion is hindered even in the presence of mechanical discontinuities. These combined effects result in a higher thermal transition temperature without a proportional gain in modulus.

Normally, there is a strong correspondence between T_g of a polymeric network and crosslinking density. By analyzing the results computed in Table 5, it can clearly be observed that the presence of GT considerably increases the crosslinking density. This sustains the active participation of the amino groups from the carbonaceous structure in the formation of supplementary interactions. Along with that, the higher values for the modulus in the rubbery plateau as compared to SP-PBz confirm the reinforcing effect of these interactions.

The "C" factor was employed to evaluate the reinforcing effect of GT, and the corresponding results are presented in Table 5. A value close to 1 for this parameter often suggests a lower efficiency of the filler. Thus, the decreased values computed for the composite systems suggest that in this case the carbon-based nanostructures have a significant influence over the properties of the materials.

The schematic representation of interactions within the ternary system illustrated in Fig. 9 is proposed based on the known chemical functionalities of the components and established literature precedents.[87–90] In the designed

nanocomposite system comprising a sesamol-derived benzoxazine/PEI matrix reinforced with carbon fibers and GT, multiple non-covalent and covalent interactions contribute to the interfacial compatibility and structural integrity. The abundant hydroxyl and amine groups from PEI, TEPA, and polybenzoxazine promote extensive hydrogen bonding throughout the matrix and at filler interfaces.[91] Aromatic structures from sesamol and graphene components enable π–π stacking with both GT and carbon fiber surfaces. Additionally, nucleophilic amine groups in PEI and TEPA may participate in covalent bonding with benzoxazine during polymerization, while dipole–dipole and potential charge–transfer interactions further enhance dispersion and load transfer. These synergistic interactions support the improved interfacial adhesion and mechanical performance of the nanocomposite.

At the same time, the carbon fibers (CF), which inherently possess oxygen-containing surface groups due to surface treatments, contribute through hydrogen bonding and π–π stacking, aiding in the physical and chemical anchoring of the matrix. The combination of CF and GT creates a multi-scale reinforcement effect, where GT acts as a nanoscopic interfacial bridge and CF offers macroscopic reinforcement. This synergistic interaction among functional groups leads to composites with improved mechanical strength and stiffness, as also reflected in the nanomechanical testing results (Fig. 13 and Table 5).

3.5. Surface properties – contact angle

Despite the high number of polar OH groups formed during ring opening polymerization, polybenzoxazines are generally characterized by hydrophobicity with low surface free energy due to the strong hydrogen bonds formed within the network.[92] Thus, besides water affinity, surface properties and wettability give valuable insights over the additional interactions formed within a material.

In this case, SP-PBz exhibits a hydrophilic character with the lowest water contact angle value of 80°. This result along with the DMA and TGA data supports the low performance of bio-based benzoxazine resin itself suggesting not only a decreased crosslinking density, but also less stable hydrogen bonds formed within the network.

The introduction of GT within the system shifts the water CA values to hydrophobicity increasing gradually as a function of graphene concentration despite the increased content of polar functional groups. These results demonstrate that the amino groups present on the surface of graphene oxide participate in the formation of additional crosslinks and hydrogen bonds that diminish the water affinity.[93]

In comparison with SP-PBz, the introduction of CF significantly modified the nature of the coating by increasing the hydrophobicity ($\sim 104°$ CA water). The prominent hydrophobic nature of carbon fibers comes from its chemical structure consisting mainly of carbon atoms.[94] However, the presence of graphene oxide in the tricomponent system alters the water-repellent behavior as a consequence of the polar groups present on its surface. As a consequence, in the case of ternary nanocomposite materials, the contact angle considerably shifts

Table 5 DMA parameters for the tricomponent nanocomposite system

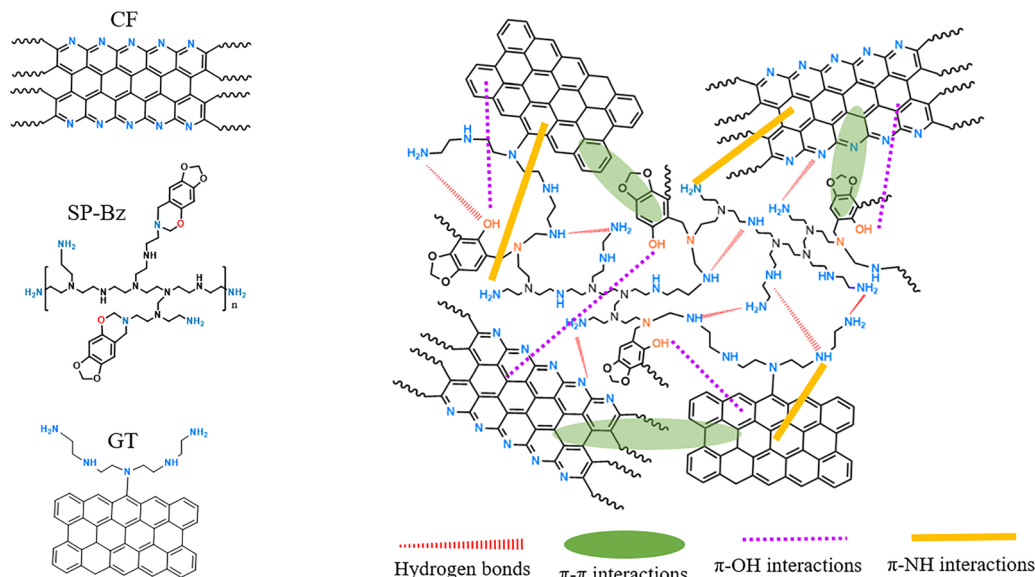| Sample	T_g (°C)	E' in the glassy state (MPa)	E' in the rubbery plateau (MPa)	$\rho_x \times 10^3$ mol cm^{-3}	C
SP-PBz	128.9	541.2	22.7	0.603	—
SP-CF-PBz	181.4	18 416.3	1051.8	4.714	1
SP-GT1-CF-PBz	188.8	20 432.1	2277.7	6.387	0.51
SP-GT2-CF-PBz	195.6	22 306.2	2528.4	6.611	0.50
SP-GT3-CF-PBz	208.1	16 814.3	2466.5	6.542	0.39

Fig. 9 Schematic representation of the possible secondary interactions formed within the tricomponent network.
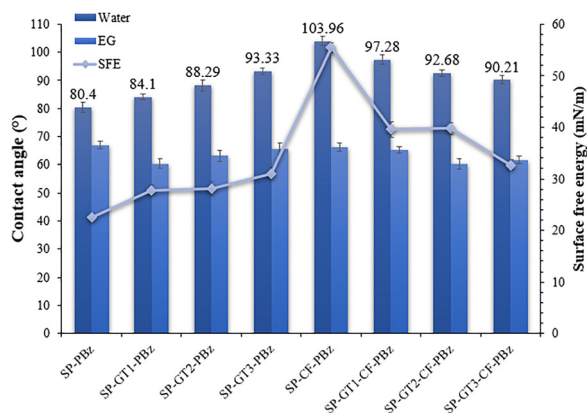

Fig. 10 Surface properties of bio-based ternary nanocomposite materials.

to hydrophilic values. We may conclude that the presence of carbon fiber within the system strongly improves the wettability, which represents a key parameter in the process of laminate composite formulation.

The surface free energy of organic nanocomposites represents a valuable parameter that can influence the overall performance as it gives insights into the interfacial interactions between the components.[95] SP-GT2-CF-PBZ has the highest value for surface free energy in comparison with the other nanocomposite formulations (39.75 mN m^{-1}) suggesting good interfacial adhesion and wettability.[96] In this case the presence of GT is associated with enhanced interfacial bonding and mechanical interlocking between the fibers and the matrix (Fig. 10).[97]

The polar nature of the polymeric matrix coming from the numerous hydroxyl groups generated during oxazine ring opening is the main reason for water absorption in composite formulations. Usually, for such composites the moisture

absorption usually takes place in two steps that strongly depend on the interfacial interactions between the matrix and the fibers. In the first step, the water molecules travel towards the inner part of the material *via* a diffusion process through the polymeric matrix as well as through the fiber interface generating multiple microcracks and voids. During the second stage water diffusion takes place mostly *via* physical processes through the structural defects formed during the first stage.[98,99]

The water absorption capacity was evaluated for the ternary nanocomposite samples and the results are presented in Fig. 11. As can be observed, the temperature exerts a significant influence over water absorption behavior. There is a considerable difference between the systems measured at 25 and 80 °C in the first 24 hours of water immersion. Higher temperatures promote faster absorption as a consequence of increased molecular motion and also favor the mobility of the polymeric chain segments creating voids within the matrix that are more susceptible to water absorption. Apart from that the high porosity of the carbon fibers along with the presence of various structural defects such as microcracks promotes water absorption.[100,101] After 3 days of immersion the initial water absorption spike determined for the systems measured at 80 °C decreased considerably due to the reorganization of the macromolecular chains.[102] Along with that the redistribution of water molecules within the material occurs after prolonged exposure to humidity as local saturation occurs at the surface of the materials providing new pathways for water diffusion.

In both cases, the humidity content increases in the ternary nanocomposites as a function of GT concentration. The additional polar groups brought by the carbon-based nanostructure tend to form more hydrogen bonds with water molecules leading to a maximum of 0.12% water uptake in both cases. However, it is possible that GT may retain some residual oxygen-containing groups, such as epoxides, hydroxyls, or
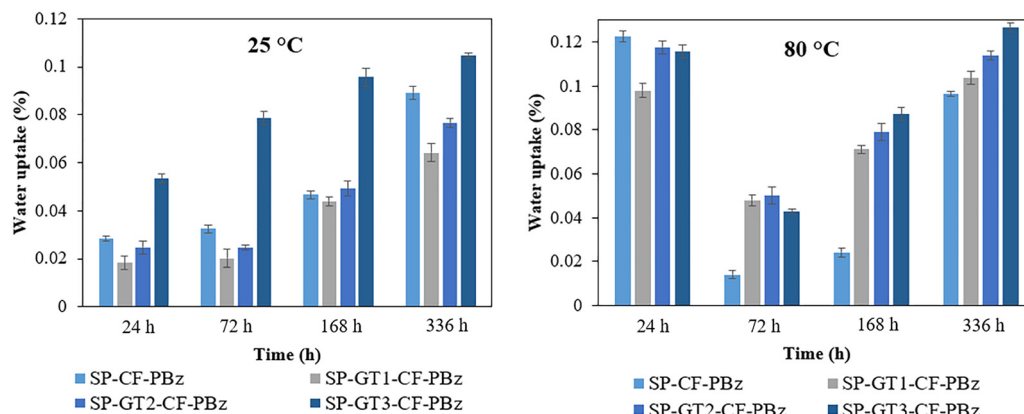
Fig. 11 Hydrothermal aging of ternary nanocomposites at 25 °C and 80 °C determined at 1, 3, 7 and 14 days.

carboxyls besides the amino groups, which have the potential to influence the long-term stability of the materials, especially under high-humidity conditions that could potentially activate these sites and affect performance.

3.6. Scanning electron microscopy

The surface morphologies of carbon fiber-graphene oxide-based laminates were analyzed *via* SEM in order to reveal the interface. The SP-CF-PBz sample from Fig. 12(a) displays the surface of the carbon fibers with small fragments of resin indicating poor compatibility between the components. Along with the gradual inclusion of GT it can clearly be observed that morphology is different, indicating a strong interfacial adhesion between the fibers and the matrix. We can assume that the aromatic structure of graphene enhances the formation of an interlocking network at the nanoscale within the system favored by physical interactions such as van der Waals forces and hydrogen bonds.[103,104]

SP-GT1-CF-PBz displays a smooth surface with a uniform dispersion of graphene nanoflakes and a reduced predisposition for agglomeration. In this case the debonding interface

suggests a strong interaction between the fibers and bio-based resin.

SP-GT2-CF-PBz displays the most uniform surface morphology among all samples. The carbon fibers are tightly embedded in the matrix, with minimal gaps or cracks. GT appears well-dispersed along the fiber surface and in the matrix, suggesting excellent fiber–matrix adhesion and GT dispersion, indicating also strong interfacial interactions likely due to optimal graphene concentration. This morphology supports enhanced mechanical properties due to efficient stress transfer and cohesive integrity of the composite structure. In the case of SP-GT3-CF-PBz a rougher surface with some aligned fibers can be noticed, also with an increase in filler aggregation. Some particles appear to be loosely attached to or even detached from the matrix. This may indicate GT agglomeration, which often occurs at higher loadings. These clusters can lead to stress concentration points and defects in the matrix that can compromise the mechanical integrity of the composite, reducing the overall performance.

3.7. Nanomechanical properties

The nanomechanical properties at the surface were recorded for each sample through nanoindentation and the corresponding results are presented in Fig. 13. The reinforcing effect of graphene flakes strongly influences nanomechanical properties of the synthesized materials. The additional chemical and physical interactions developed between the numerous functional groups present on the surface of the carbonaceous nanostructure and the other components of the systems improve not only the stiffness but also high load-bearing capacity.[105] Thus, introduction of GT in the SP-CF-PBz samples leads to a strengthening effect *via* creation of an interface between the carbon fibers and the polybenzoxazine matrix through mechanical interlocking.[97]

Results plotted for a 900–1000 nm indentation depth presented in Fig. 13b show no significant difference when comparing SP-CF-PBz ($E = 1.03 \pm 0.12$ GPa, $H = 0.08 \pm 0.01$ GPa) and SP-GT1-CF-PBz ($E = 1.33 \pm 0.06$ GPa, $H = 0.11 \pm 0.02$ GPa). A sharp increase in both modulus and hardness occurred for the SP-GT2-CF-PBz sample ($E = 6.10 \pm 0.46$ GPa, $H = 0.36 \pm 0.06$ GPa), confirming the reinforcing effect of GT at 2% concentration. These results are in agreement with DMA results.
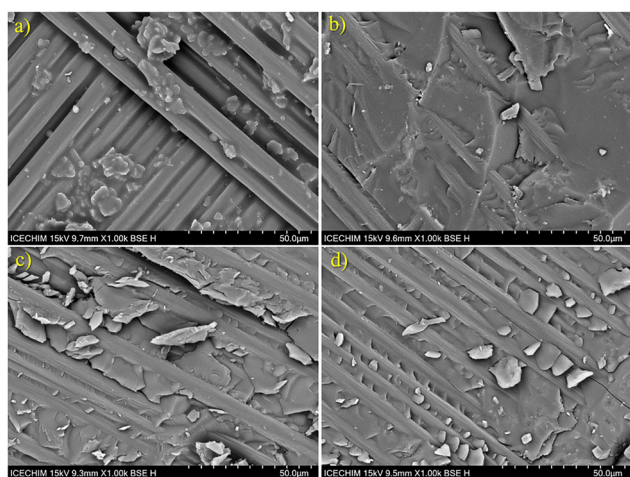

Fig. 12 SEM micrographs of (a) SP-CF-PBZ, (b) SP-GT1-CF-PBz, (c) SP-GT2-CF-PBz, and (d) SP-GT3-CF-PBz nanocomposites.
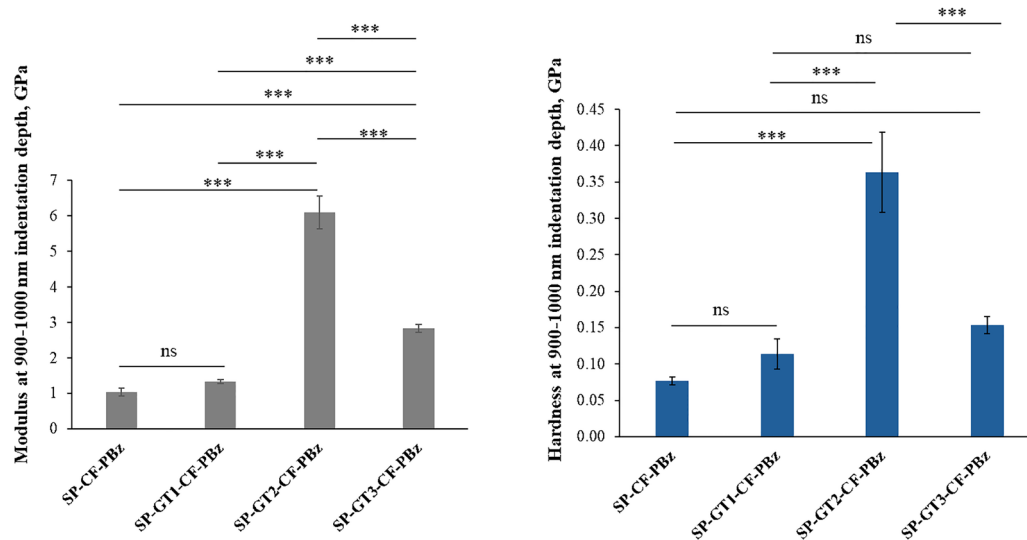
Fig. 13 Nanomechanical results for bio-based ternary nanocomposite systems measured by nanoindentation. Statistical significance: ns – not significant, *$p < 0.05$, **$p < 0.01$, ***$p < 0.001$, ****$p < 0.0001$.

The considerable diminishing in nanomechanical properties for SP-GT3-CF-PBz sample confirms that at 3% loading, the graphene nanoflakes have a high tendency to form agglomerates that will further become weak points with a high stress concentration within the material.

3.8. Electromagnetic (EM) shielding

Fig. 14 displays the experimental results for the materials under test (MUTs) in terms of SE_A, SE_R, and SE, between 8 and 12 GHz, for the reference MUT (SP-CF-PBZ, solid black curve, no GT content) and three other MUTs with a content of GT equal to
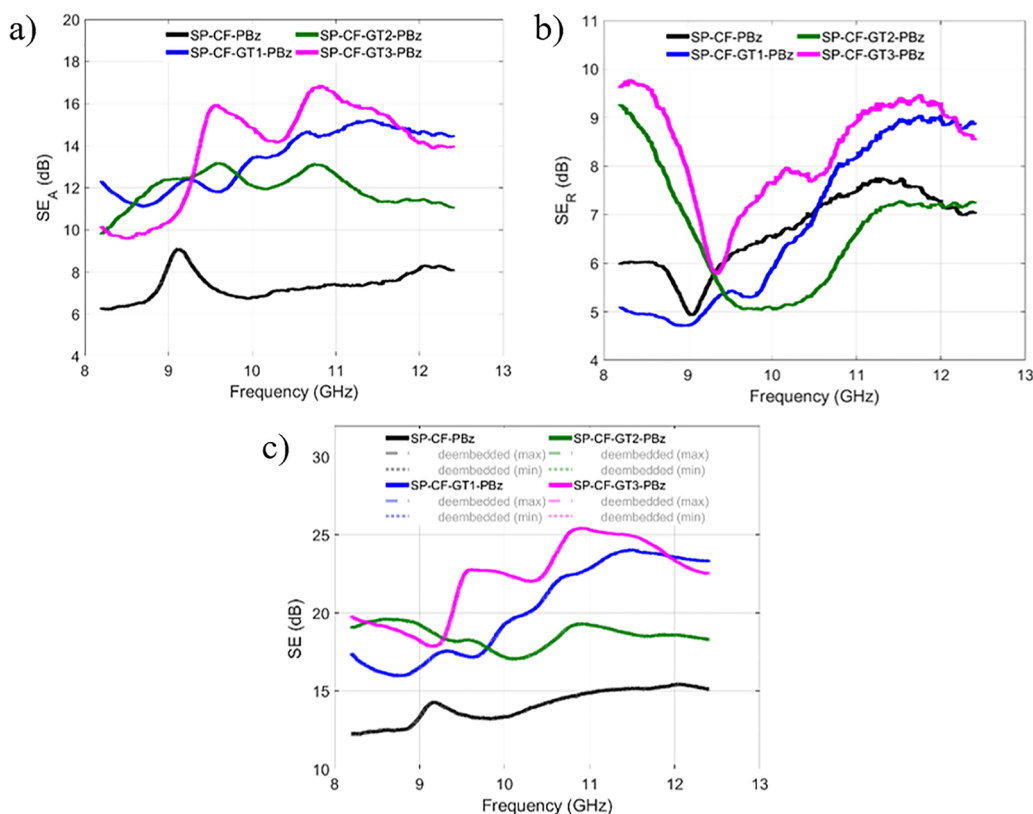
Fig. 14 Extracted (a) SE_A, (b) SE_R, and (c) SE between 8 and 12 GHz, for the reference SP-CF-PBz (solid black curve, no GT content) and three other SP-CF-PBz nanocomposites with a content of GT equal to 1% (solid blue curve), 2%, (solid green curve), and 3% (solid pink curve).

Table 6 Average over the whole X band of the extracted material parameters

Sample	ε'_r	ε''_r	μ'_r	μ''_r	σ (S m^{-1})
SP-CF-PBz	76.2	25.2	1.01	0.36	14.4
SP-CF-GT1-PBz	116.8	16.6	0.65	0.65	9.5
SP-CF-GT2-PBz	92.9	57.4	1.05	0.41	32.8
SP-CF-GT3-PBz	150.2	70.9	0.87	0.72	40.5

are shown). The NRW procedure applied for this smoothed de-embedded curve led to the other results shown in the same figure, *i.e.*, the complex permittivity (real part – top right, imaginary part – bottom left) and the equivalent conductivity computed from the permittivity (bottom right). Table 6 holds average values over the whole X band. The results reflect the average behavior of the samples, which have different absorption/reflection properties, depending on the frequency. In detail, the dielectric constant (*i.e.*, real part of the complex permittivity) spans the range between 70 and 160 in the 8–12 GHz range, which reflects a strong absorption mechanism. On the other hand, the conductivity attains maximum values between 30 and 45 S m^{-1} (SP-CF-GT3-PBz), which are quite high for such a nanocomposite system based on functionalized graphene oxide, carbon fibers and bio-based polybenzoxazine.

The EMI shielding behavior of the SP-GT-CF-PBz composite can be attributed to several synergistic mechanisms. The integration of conductive carbon fibers and TEPA-functionalized rGO creates a multiscale conductive network that facilitates electron transport and conductive loss. Furthermore, the strong interfacial interactions and high density of heteroatom-rich interfaces contribute to interfacial polarization, enhancing dielectric loss through Maxwell–Wagner–Sillars effects. The presence of residual functional groups on rGO and polar amines from TEPA introduces dipolar polarization centers, which further absorb electromagnetic radiation. The hierarchical structure and good dispersion of nanofillers also promote multiple reflection and scattering of waves within the composite, increasing the overall shielding effectiveness.[106–110] These combined mechanisms support the efficient attenuation of EM waves through absorption-dominated processes.

4. Conclusions

Ternary nanocomposite laminates based on the bio-based benzoxazine monomer, carbon fibers and different loadings of GT were successfully synthesized and characterized. Curing kinetics and dynamics revealed a complex crosslinking process that evolved in two distinct stages as a consequence of the catalytic effect of amino functionalities present on the backbone of the benzoxazine monomer. DSC results revealed that the presence of GT nanoflakes influenced the dynamic of the process as a function of concentration as evidenced by both crosslinking density values and activation energy.

SP-PBz shows good thermal resistance with a $T_{d5\%}$ of around 238 °C. The introduction of GT reduces the resistance slightly in the nanocomposite at 1%, but the SP-GT2-PBz sample offers the optimum resistance. As expected, the presence of CF considerably increases $T_{d5\%}$ that reaches ∼300 °C and residual mass which improves the thermal stability and flame resistance of the laminates.

DMA results evidenced that both GT and carbon fibers contribute significantly to the improvement of the poor inherent mechanical properties of the polybenzoxazine matrix. Thus, the storage modulus of SP-GT2-CF-PBz increases up to 340-fold compared to pure SP-PBz. Apart from that, GT also influences the T_g which increases with the addition of graphene, reaching 208 °C for SP-GT3-CF-PBz. Compared to the neat PBz matrix, the ternary nanocomposite containing 2 wt% GT shows an approximate 98% increase in the storage modulus and exhibits an around 22% higher modulus than the SP-CF-PBz composite.

Nanomechanical tests revealed that the optimum concentration of GT in the ternary nanocomposites at which the properties are significantly increased is 2%. Thus, the modulus of SP-GT2-CF-PBz increases by ∼83% in comparison with SP-CF-PBz and hardness for the same nanocomposite with ∼78%. However, a 3% GT loading leads to the formation of agglomerates, reducing the mechanical properties and introducing weaknesses in the material, as also sustained by the SEM analysis.

Surface properties of the ternary nanocomposites revealed that both graphene oxide nanoflakes and carbon fibers influence surface properties. SP-GT2-CF-PBZ shows the highest surface energy (39.75 mN m^{-1}), indicating good interfacial adhesion while SP-GT3-CF-PBZ exhibits the most significant EM shielding behavior. The EMI shielding properties of the proposed nanocomposite system represent the state-of-the-art in the domain of carbon-based materials for EMI shielding applications. SP-GT3-CF-PBz composite has superior performance in terms of shielding effectiveness in the X band with respect to other carbon-based materials, with a much lower thickness. Furthermore, the new nanocomposite is bio-based, flexible but also robust, and thermally stable up to 240 degrees, which makes it suitable for many industrial and commercial applications.

The proposed ternary nanocomposite systems show an improvement in both mechanical and thermal properties as a result of the chemical binding of GT to the benzoxazine matrix and to the π–π interactions between carbon fibers, graphene and the benzoxazine. The free amino groups from both benzoxazine monomer and graphene oxide surface may generate an active interface between the components of the systems leading to superior thermal and mechanical performance.

While the present study demonstrates promising mechanical and thermal performance of SP-GT-CF-PBz nanocomposites, further studies are needed to assess the long-term stability and durability under operational environments. In addition, the functionalization and fabrication approaches, while effective at the lab scale, require optimization for industrial scalability.

Conflicts of interest

There are no conflicts to declare.

Data availability

The raw data required to reproduce these findings can be shared upon request.

Acknowledgements

References

1 C.-M. Lin, C.-H. Chen, C.-H. Lin and T.-Y. Juang, High-performance bio-based benzoxazines derived from phosphinated biphenols and furfurylamine, *Eur. Polym. J.*, 2018, **108**, 48–56.

2 S. Gulyuz and B. Kiskan, Combination of Polyethylenimine and Vanillin-Based Benzoxazine as a Straightforward Self-Healable System with Excellent Film-Forming Ability, *Macromolecules*, 2024, **57**(5), 2078–2089.

3 X. Liu, Z. Li, G. Zhan, Y. Wu and Q. Zhuang, Bio-based benzoxazines based on sesamol: Synthesis and properties, *J. Appl. Polym. Sci.*, 2019, **136**(48), 48255.

4 K. M. Mydeen, H. Arumugam, B. Krishnasamy and A. Muthukaruppan, Sesamol-based polybenzoxazines for ultra-low-k, high-k and hydrophobic coating applications, *New J. Chem.*, 2023, **47**(16), 7873–7889.

5 H. Yao, X. Lu, Z. Xin, X. Li, C. Chen and Y. Cao, Two novel eugenol-based difunctional benzoxazines: Synthesis and properties, *Colloids Surf., A*, 2021, **616**, 126209.

6 L. Dumas, L. Bonnaud, M. Olivier, M. Poorteman and P. Dubois, Eugenol-based benzoxazine: from straight synthesis to taming of the network properties, *J. Mater. Chem. A*, 2015, **3**(11), 6012–6018.

7 D. Apostolidis, L. F. G. Noleto, W. E. Dyer, I. F. Teixeira and B. Kumru, m-Guaiacol-Derived Benzoxazine Resins as Surprising Heterogeneous Photocatalysts for the Photocatalytic Production of Hydrogen Peroxide under Visible Light, *Artif. Photosynth.*, 2024, **1**, 134–143.

8 A. Adjaoud, L. Puchot, C. E. Federico, R. Das and P. Verge, Lignin-based benzoxazines: A tunable key-precursor for the design of hydrophobic coatings, fire resistant materials and catalyst-free vitrimers, *Chem. Eng. J.*, 2023, **453**, 139895.

9 H. Arumugam, S. Krishnan, M. Chavali and A. Muthukaruppan, Cardanol based benzoxazine blends and bio-silica reinforced composites: thermal and dielectric properties, *New J. Chem.*, 2018, **42**(6), 4067–4080.

10 X. Wang, H. Niu, J. Huang, L. Song and Y. Hu, A desoxyanisoin- and furfurylamine-derived high-performance benzoxazine thermoset with high glass transition temperature and excellent anti-flammability, *Polym. Degrad. Stab.*, 2021, **189**, 109604.

11 H. A. Klfout, A. M. Asiri, K. A. Alamry and M. A. Hussein, Recent advances in bio-based polybenzoxazines as an interesting adhesive coating, *RSC Adv.*, 2023, **13**(29), 19817–19835.

12 K. I. Aly, M. G. Mohamed, O. Younis, M. H. Mahross, M. Abdel-Hakim and M. M. Sayed, Salicylaldehyde azine-functionalized polybenzoxazine: Synthesis, characterization, and its nanocomposites as coatings for inhibiting the mild steel corrosion, *Prog. Org. Coat.*, 2020, **138**, 105385.

13 N. Furukawa, K. Kawasaki, K. Imura, T. Ureshino, M. Yamamoto and T. Takeichi, Thermal and Mechanical Properties of Newly Developed Poly-functional Benzoxazine, *J. Adhes. Soc. Jpn.*, 2007, **43**, 89–96.

14 Y. Tang, H. E. Symons, P. Gobbo, J. S. Van Duijneveldt, I. Hamerton and S. Rochat, Properties and Curing Kinetics of a Processable Binary Benzoxazine Blend, *ACS Appl. Polym. Mater.*, 2023, **5**(12), 10404–10415.

15 C. Hu, Z. Yao, W. Zhao and K. Zhang, Synthesis, Characterization, and Structure–Property Investigations of Benzoxazine Resins with Low Surface Free Energy, *Macromol. Chem. Phys.*, 2025, **226**, 2400152.

16 S. A. Gârea, C. Andronescu and H. Iovu, Chapter 40 - Polybenzoxazine-Clay Nanocomposites. in *Advanced and Emerging Polybenzoxazine Science and Technology*, ed. H. Ishida and P. Froimowicz, Elsevier, Amsterdam, 2017, pp. 835–859.

17 M. G. Mohamed, A. Mahdy, R. J. Obaid, M. A. Hegazy, S.-W. Kuo and K. I. Aly, Synthesis and characterization of polybenzoxazine/clay hybrid nanocomposites for UV light shielding and anti-corrosion coatings on mild steel, *J. Polym. Res.*, 2021, **28**(8), 297.

18 I. Biru, C. M. Damian, S. A. Gârea and H. Iovu, Benzoxazine-functionalized graphene oxide for synthesis of new nanocomposites, *Eur. Polym. J.*, 2016, **83**, 244–255.

19 S. Sahila, A. Chhonkar and L. Jayakumari, Graphene Oxide – Cardanol Based Polymer Benzoxazine Nanocom-Posite as High Dielectric Strength Material for Electrical Applications, *Adv. Compos. Lett.*, 2015, **24**, 21–26.

20 M. Zeng, J. Wang, R. Li, J. Liu, W. Chen, S. Q. Xu and Y. Gu, The curing behavior and thermal property of graphene oxide/benzoxazine nanocomposites, *Polymer*, 2013, **54**, 3107–3116.

21 S. Zachariah and Y.-L. Liu, Nanocomposites of polybenzoxazine-functionalized multiwalled carbon nanotubes and polybenzoxazine for anticorrosion application, *Compos. Sci. Technol.*, 2020, **194**, 108169.

22 Y.-J. Hu, Y. Wang, Y.-H. Huang, J. Bian, M.-F. Li, F. Peng and R.-C. Sun, Benzoxazine enhanced amino cellulose-based composite films: Preparation, proposed mechanism, and improved performance, *Carbohydr. Polym.*, 2019, **222**, 115008.

23 T. Agag, K. Vietmeier, A. Chernykh and H. Ishida, Side-chain type benzoxazine-functional cellulose via click chemistry, *J. Appl. Polym. Sci.*, 2012, 125.

24 R. Rajamanikam, P. Pichaimani, M. Kumar and A. Muthukaruppan, Optical and thermomechanical behavior of benzoxazine functionalized ZnO reinforced poly-benzoxazine nanocomposites, *Polym. Compos.*, 2017, **38**(9), 1881–1889.

25 M. Wan Hassan, J. Liu, B. Howlin, H. Ishida and I. Hamerton, Examining the influence of bisphenol A on the polymerisation and network properties of an aromatic benzoxazine, *Polymer*, 2016, 88.

26 P. Sharma and L. Nebhani, Expanding the library of nitrogen enriched polybenzoxazine thermosets prepared from side-chain type benzoxazines functionalized with polyethylenimine, *Eur. Polym. J.*, 2021, **155**, 110542.

27 M. I. Necolau, I. E. Bîru, J. Ghitman, C. Stavarache and H. Iovu, Insightful characterization of sesamol-based poly-benzoxazines: Effect of phenol and amine chain type on physical and nanomechanical properties, *Polym. Test.*, 2022, **110**, 107578.

28 S. Pilato, S. Moffa, G. Siani, F. Diomede, O. Trubiani, J. Pizzicannella, D. Capista, M. Passacantando, P. Samorì and A. Fontana, 3D Graphene Oxide-Polyethylenimine Scaffolds for Cardiac Tissue Engineering, *ACS Appl. Mater. Interfaces*, 2023, **15**(11), 14077–14088.

29 J. Zong and Q. Ran, Ring Opening Reaction of 3,4-Dihydro-2H-1,3-Benzoxazine with Amines at Room Temperature, *ChemistrySelect*, 2019, **4**(22), 6687–6696.

30 T. Agag, C. R. Arza, F. H. J. Maurer and H. Ishida, Primary Amine-Functional Benzoxazine Monomers and Their Use for Amide-Containing Monomeric Benzoxazines, *Macromolecules*, 2010, **43**(6), 2748–2758.

31 S. Zhang, J. Zong, Q. Ran and Y. Gu, Facile Preparation of Lightweight and Robust Polybenzoxazine Foams, *Ind. Eng. Chem. Res.*, 2020, **59**(16), 7575–7583.

32 J. Sun, W. Wei, Y. Xu, J. Qu, X. Liu and T. Endo, A curing system of benzoxazine with amine: reactivity, reaction mechanism and material properties, *RSC Adv.*, 2015, **5**(25), 19048–19057.

33 B. A. Newcomb, Processing, structure, and properties of carbon fibers, *Composites, Part A*, 2016, **91**, 262–282.

34 J. Zhang, G. Lin, U. Vaidya and H. Wang, Past, present and future prospective of global carbon fibre composite developments and applications, *Composites, Part B*, 2023, **250**, 110463.

35 B. Salahuddin, S. N. Faisal, T. A. Baigh, M. N. Alghamdi, M. S. Islam, B. Song, X. Zhang, S. Gao and S. Aziz, Carbonaceous Materials Coated Carbon Fibre Reinforced Polymer Matrix Composites, *Polymers*, 2021, **13**(16), 2771.

36 C. Y. X. Chua, H.-C. Liu, N. Di Trani, A. Susnjar, J. Ho, G. Scorrano, J. Rhudy, A. Sizovs, G. Lolli, N. Hernandez, M. C. Nucci, R. Cicalo, M. Ferrari and A. Grattoni, Carbon fiber reinforced polymers for implantable medical devices, *Biomaterials*, 2021, **271**, 120719.

37 A. Zotti, S. Zuppolini, A. Borriello, L. Trinchillo, V. Vinti and M. Zarrelli, Hierarchical aerospace epoxy composites of carbon fiber and hyperbranched filler: toughening behavior from nanocomposites to composites, *Compos. Struct.*, 2024, **327**, 117719.

38 B. Rijo, A. P. S. Dias and J. P. S. Carvalho, Recovery of carbon fibers from aviation epoxy composites by acid solvolysis, *Sustainable Mater. Technol.*, 2023, **35**, e00545.

39 R. Patole, N. Ambhore and D. Agrawal, Carbon Composites in Aerospace Application -A Comprehensive Review, *Mater. Int.*, 2023, **5**, 12.

40 R. Gholami, A. R. Khoogar and M. H. Allaei, Optimizing mechanical performance: Epoxy-graphene oxide nanocomposites for enhanced strength in lattice structure, *Heliyon*, 2025, **11**(2), e41576.

41 M. Mirzapour; M. Robert and B. Benmokrane, *In Situ Processing to Achieve High-Performance Epoxy Nanocomposites with Low Graphene Oxide Loading C*, 2024.

42 J. An, Y. Zhang, X. Zhang, M. He, J. Zhou, J. Zhou, Y. Liu, X. Chen, Y. Hu, X. Song, J. Chen, T. Wu, J. Kang and Z. Xie, Structure and Properties of Epoxy Resin/Graphene Oxide Composites Prepared from Silicon Dioxide-Modified Graphene Oxide, *ACS Omega*, 2024, **9**(15), 17577–17591.

43 P. Singh, S. Sharma, K. Kumar, G. Iyer and A. Kumar, A Comparative Study on Mechanical Properties of Yttrium Oxide and Reduced Graphene Oxide Reinforced Epoxy Nanocomposites, *J. Mater. Eng. Perform.*, 2025, **34**(5), 3706–3716.

44 P. Saini and M. Arora, Microwave Absorption and EMI Shielding Behavior of Nanocomposites Based on Intrinsically Conducting Polymers, Graphene and Carbon Nanotubes, *In New Polymers for Special Applications*, ed. A. De Souza Gomes, IntechOpen, Rijeka, 2012.

45 A. Kausar, I. Ahmad, T. Zhao, O. Aldaghri, K. H. Ibnaouf, M. H. Eisa and T. D. Lam, Graphene Nanocomposites for Electromagnetic Interference Shielding—Trends and Advancements, *J. Compos. Sci.*, 2023, **7**, 384.

46 Z.-X. Chen, C. Chang, X. Yue, H. Li, C.-G. Liang and P.-C. Ma, Experimental and theoretical study on the electromagnetic shielding performance of polymer nanocomposites consisting of basalt fiber and CNTs, *Compos. Sci. Technol.*, 2024, **247**, 110399.

47 F. Shahzad, M. Alhabeb, C. B. Hatter, B. Anasori, S. Man Hong, C. M. Koo and Y. Gogotsi, Electromagnetic interference shielding with 2D transition metal carbides (MXenes), *Science*, 2016, **353**(6304), 1137–1140.

48 Y. Gan and Y. Xiong, Review of MXene synthesis and applications in electromagnetic shielding, *RSC Adv.*, 2025, **15**(12), 9555–9568.

49 Y. Liu, Y. Liu and X. Zhao, MXene Composite Electromagnetic Shielding Materials: The Latest Research Status, *ACS Appl. Mater. Interfaces*, 2024, **16**(31), 41596–41615.

50 E. Rusen, A. Mocanu, G. Toader, A. Diacon, C. Romanitan, O. Iorga, M. Aldrigo, C. Parvulescu, R. Mitran and

O. Brincoveanu, Design of polyurethane composite foam obtained from industrial PET wastes and MXenes for EMI shielding applications, *RSC Adv.*, 2024, **14**(50), 37202–37215.

51 E. Rusen, A. Mocanu, O. Brincoveanu, A. Boldeiu, C. Romanitan, M. Aldrigo, S. Iordănescu, A. Diacon, G. Toader and R. Gavrila, MXenes and polymeric colloids nanocomposites for EMI shielding, *J. Mater. Chem. C*, 2024, **12**(30), 11586–11593.

52 E. Rusen, A. Mocanu, A. Dinescu, A. Boldeiu, C. Romanitan, S. Iordanescu, M. Aldrigo, R. Somoghi, R. Mitran and A. Ghebaur, Different morphologies of super-balls obtained to form photonic crystals of cholesteryl benzoate liquid crystals, *Nanoscale Adv.*, 2024, **6**(19), 4814–4824.

53 J. Fan, J. Yang, L. Wang, H. Li, J. Tian, J. Ye and Y. Zhao, Enhanced mechanical properties of epoxy nanocomposites with mildly surface-functionalized graphene oxide by tuned amine species, *Appl. Surf. Sci.*, 2021, **558**, 149964.

54 M. Song and J. Xu, Preparation of Polyethylenimine-Functionalized Graphene Oxide Composite and Its Application in Electrochemical Ammonia Sensors, *Electroanalysis*, 2013, **25**(2), 523–530.

55 H. Kim, A. A. Abdala and C. W. Macosko, Graphene/Polymer Nanocomposites, *Macromolecules*, 2010, **43**(16), 6515–6530.

56 Q. Liu, Y. Zhao, S. Gao, X. Yang, R. Fan, M. Zhi and M. Fu, Recent advances in the flame retardancy role of graphene and its derivatives in epoxy resin materials, *Composites, Part A*, 2021, **149**, 106539.

57 I. Collado, A. Jiménez-Suárez, A. Vázquez-López, G. del Rosario and S. G. Prolongo, Ultrasonication Influence on the Morphological Characteristics of Graphene Nanoplatelet Nanocomposites and Their Electrical and Electromagnetic Interference Shielding Behavior, *Polymers*, 2024, **16**, 1068.

58 M. I. Necolau, I. N. Radu, B. Bălănucă, A. N. Frone and C. M. Damian, Broadening the coating applications of sustainable materials by reinforcing epoxidized corn oil with single-walled carbon nanotubes, *Environ. Sci. Pollut. Res.*, 2024, **31**(25), 37465–37479.

59 M. Yuan, X. Lu, X. Ma, H. Lin, A. Lu, L. Shao and Z. Xin, Polybenzoxazine/organosilicon composites with low dielectric constant and dielectric loss, *Chin. J. Chem. Eng.*, 2023, **64**, 241–249.

60 J. Jyoti, B. P. Singh, A. K. Arya and S. R. Dhakate, Dynamic mechanical properties of multiwall carbon nanotube reinforced ABS composites and their correlation with entanglement density, adhesion, reinforcement and C factor, *RSC Adv.*, 2016, **6**(5), 3997–4006.

61 D. W. van Krevelen, Some basic aspects of flame resistance of polymeric materials, *Polymer*, 1975, **16**(8), 615–620.

62 K. Zhang, W. Liang, F. Wang and Z. Wang, Effect of water absorption on the mechanical properties of bamboo/glass-reinforced polybenzoxazine hybrid composite, *Polym. Polym. Compos.*, 2021, **29**, 096739112090366.

63 V. García-Martínez, M. R. Gude, S. Calvo and A. Ureña, Enhancing an Aerospace Grade Benzoxazine Resin by Means of Graphene Nanoplatelets Addition, *Polymers*, 2021, **13**(15), 2544.

64 S. Rehman, S. Akram, A. Kanellopoulos, A. Elmarakbi and P. G. Karagiannidis, Development of new graphene/epoxy nanocomposites and study of cure kinetics, thermal and mechanical properties, *Thermochim. Acta*, 2020, **694**, 178785.

65 V. V. Shutov, N. V. Bornosuz, R. F. Korotkov, I. Y. Gorbunova and I. S. Sirotin, Kinetics of benzoxazine and epoxy oligomer copolymerization, *Thermochim. Acta*, 2022, **714**, 179254.

66 A. Ručigaj, Š. Gradišar and M. Krajnc, Kinetic investigation of a complex curing of the guaiacol bio-based benzoxazine system, *e-Polymers*, 2016, **16**(3), 199–206.

67 X. Chen, W. Jiang, B. Hu, Z. Liang, Y. Zhang, J. Kang, Y. Cao and M. Xiang, Effects of graphene oxide size on curing kinetics of epoxy resin, *RSC Adv.*, 2021, **11**(47), 29215–29226.

68 V. García-Martínez, M. R. Gude, S. Calvo, M. R. Martínez-Miranda and A. Ureña, Influence of graphene nanoplatelets on curing kinetics and rheological properties of a benzoxazine resin, *Mater. Today Commun.*, 2020, **24**, 100990.

69 N. Sbirrazzuoli, Advanced Isoconversional Kinetic Analysis for the Elucidation of Complex Reaction Mechanisms: A New Method for the Identification of Rate-Limiting Steps, *Molecules*, 2019, **24**, 1683.

70 A. Toldy, G. Szebényi, K. Molnár, L. F. Tóth, B. Magyar, V. Hliva, T. Czigány and B. Szolnoki, The Effect of Multi-level Carbon Reinforcements on the Fire Performance, Conductivity, and Mechanical Properties of Epoxy Composites, *Polymers*, 2019, **11**, 303.

71 Q. Qu, J. Xu, H. Wang, Y. Yu, Q. Dong, X. Zhang and Y. He, Carbon Nanotube-Based Intumescent Flame Retardants Achieve High-Efficiency Flame Retardancy and Simultaneously Avoid Mechanical Property Loss, *Polymers*, 2023, **15**, 1406.

72 A. L. Higginbotham, J. R. Lomeda, A. B. Morgan and J. M. Tour, Graphite Oxide Flame-Retardant Polymer Nanocomposites, *ACS Appl. Mater. Interfaces*, 2009, **1**(10), 2256–2261.

73 P. Paraskar, P. Bari and S. Mishra, Influence of amine functionalized graphene oxide on mechanical and thermal properties of epoxy matrix composites, *Iran. Polym. J.*, 2019, **29**.

74 A. Kowalczyk, M. Tokarczyk, M. Weisbrodt and K. Gziut, Adhesive Films Based on Benzoxazine Resins and the Photoreactive Epoxyacrylate Copolymer, *Materials*, 2022, **15**, 1839.

75 S. S. Rishwana, A. Mahendran and C. Vijayakumar, Studies on structurally different benzoxazines:Curing characteristics and thermal degradation aspects, *High Perform. Polym.*, 2015, **27**(7), 802–812.

76 B. Mensah, D. S. Konadu, F. Nsaful, P. N. Angnunavuri and S. Kwofie, A systematic study of the effect of graphene oxide and reduced graphene oxide on the thermal degradation behavior of acrylonitrile-butadiene rubber in air and nitrogen media, *Sci. Afr.*, 2023, **19**, e01501.

77 M. Mirza-Aghayan, M. Mohammadi, A. Addad and R. Boukherroub, Pd nanoparticles supported on reduced graphene oxide as an effective and reusable heterogeneous catalyst for the Mizoroki–Heck coupling reaction, *Appl. Organomet. Chem.*, 2020, **34**(4), e5524.

78 P. Luengrojanakul, P. Mora, K. Bunyanuwat, C. Jubsilp and S. Rimdusit, Improvements in Mechanical and Shape-Memory Properties of Bio-Based Composite: Effects of Adding Carbon Fiber and Graphene Nanoparticles, *Polymers*, 2023, **15**, 4513.

79 N. Mattar, V. Langlois, E. Renard, T. Rademacker, F. Hübner, M. Demleitner, V. Altstädt and H. Ruckdäschel, Rios de Anda, A., Fully Bio-Based Epoxy-Amine Thermosets Reinforced with Recycled Carbon Fibers as a Low Carbon-Footprint Composite Alternative, *ACS Appl. Polym. Mater.*, 2021, **3**(1), 426–435.

80 C. Boursier Niutta, R. Ciardiello, A. Tridello and D. S. Paolino, Epoxy and Bio-Based Epoxy Carbon Fiber Twill Composites: Comparison of the Quasi-Static Properties, *Materials*, 2023, **16**, 1601.

81 X. Zhou, M. Shen, F. Fu, Q. Li, H. Liu and Z. Song, High strength, self-healing and hydrophobic fully bio-based polybenzoxazine reinforced pine oleoresin-based vitrimer and its application in carbon fiber reinforced polymers, *Chem. Eng. J.*, 2024, **484**, 149585.

82 L. A. Pothan, Z. Oommen and S. Thomas, Dynamic mechanical analysis of banana fiber reinforced polyester composites, *Compos. Sci. Technol.*, 2003, **63**(2), 283–293.

83 W. Bauhofer and J. Z. Kovacs, A review and analysis of electrical percolation in carbon nanotube polymer composites, *Compos. Sci. Technol.*, 2009, **69**(10), 1486–1498.

84 I. Balberg, Tunneling and nonuniversal conductivity in composite materials, *Phys. Rev. Lett.*, 1987, **59**(12), 1305–1308.

85 E. W. Fenta and B. A. Mebratie, Advancements in carbon nanotube-polymer composites: Enhancing properties and applications through advanced manufacturing techniques, *Heliyon*, 2024, **10**(16), e36490.

86 A. Redondo, N. Mortensen, K. Djeghdi, D. Jang, R. D. Ortuso, C. Weder, L. T. J. Korley, U. Steiner and I. Gunkel, Comparing Percolation and Alignment of Cellulose Nanocrystals for the Reinforcement of Polyurethane Nanocomposites, *ACS Appl. Mater. Interfaces*, 2022, **14**(5), 7270–7282.

87 P. Mora, C. Jubsilp, C. W. Bielawski and S. Rimdusit, Impact Response of Aramid Fabric-Reinforced Polybenzoxazine/Urethane Composites Containing Multiwalled Carbon Nanotubes Used as Support Panel in Hard Armor, *Polymers*, 2021, **13**, 2779.

88 T. Periyasamy, S. P. Asrafali and S.-C. Kim, Bio-Based Polybenzoxazine–Cellulose Grafted Films: Material Fabrication and Properties, *Polymers*, 2023, **15**, 849.

89 P. Zhao, X. Liang, J. Chen, Q. Ran and Y. Gu, Poly(ether imide)-modified benzoxazine blends: Influences of phase separation and hydrogen bonding interactions on the curing reaction, *J. Appl. Polym. Sci.*, 2013, **128**(5), 2865–2874.

90 Q. Xu, M. Zeng, Z. Feng, D. Yin, Y. Huang, Y. Chen, C. Yan, R. Li and Y. Gu, Understanding the effects of carboxylated groups of functionalized graphene oxide on the curing behavior and intermolecular interactions of benzoxazine nanocomposites, *RSC Adv.*, 2016, **6**(37), 31484–31496.

91 E. I. Bîru, S. A. Gârea, A. Nicolescu, E. Vasile and H. Iovu, Advanced Polybenzoxazine Structures Based on Modified Reduced Graphene Oxide, *Polymers*, 2018, **10**(9), 941.

92 I. S. Sirotin, I. A. Sarychev, V. V. Vorobyeva, A. A. Kuzmich, N. V. Bornosuz, D. V. Onuchin, I. Y. Gorbunova and V. V. Kireev, Synthesis of Phosphazene-Containing, Bisphenol A-Based Benzoxazines and Properties of Corresponding Polybenzoxazines, *Polymers*, 2020, **12**, 1225.

93 D. Mao, X. Wang, Y. Wu, Z. Gu, C. Wang and Y. Tu, Unexpected hydrophobicity on self-assembled monolayers terminated with two hydrophilic hydroxyl groups, *Nanoscale*, 2021, **13**(46), 19604–19609.

94 B.-H. Kim, D. H. Lee, K. S. Yang, B.-C. Lee, Y. A. Kim and M. Endo, Electron Beam Irradiation-Enhanced Wettability of Carbon Fibers, *ACS Appl. Mater. Interfaces*, 2011, **3**(2), 119–123.

95 Q. Chen, H. Zhang, H. Liu, J. Yuan, Y. Gao, C. Wu, Q. Wang, G. Zhao and Y. Liu, Improved mechanical properties of carbon fiber/epoxy composites via fiber surface grafting of rigid-flexible chain structure, *Diamond Relat. Mater.*, 2024, **142**, 110739.

96 C. J. Warren and D. E. Hirt, Carbon fiber surface properties and their effect on composite performance (NASA Contractor Report 178340), NASA, 1987, Retrieved from https://ntrs.nasa.gov/api/citations/19870016001/downloads/19870016001.pdf, pp. 43–68.

97 K. Xiong, F. Liu, T. Chen and L. Xiong, Facile and efficient grafting of graphene oxide onto carbon fiber with hyperbranched poly(thioether-yne) via click chemistry to improve interface and mechanical properties of composite, *Surf. Interfaces*, 2024, **46**, 104038.

98 Y.-F. Niu, Y. Yan and J.-W. Yao, Hygrothermal aging mechanism of carbon fiber/epoxy resin composites based on quantitative characterization of interface structure, *Polym. Test.*, 2021, **94**, 107019.

99 L.-R. Bao and A. F. Yee, Moisture diffusion and hygrothermal aging in bismaleimide matrix carbon fiber composites—part I: uni-weave composites, *Compos. Sci. Technol.*, 2002, **62**(16), 2099–2110.

100 K. Xiao, Y. Fang, Z. Wang, N. Ni, Z. Liu, S. Kim, Z. An, Z. Lyu, Y. Xu and X. Yang, Bio-Sourced, High-Performance Carbon Fiber Reinforced Itaconic Acid-Based Epoxy Composites with High Hygrothermal Stability and Durability, *Polymers*, 2024, **16**, 1649.

101 W. Zuo, Q. Luo, Q. Li and G. Sun, Effect of thermal and hydrothermal aging on the crashworthiness of carbon fiber reinforced plastic composite tubes, *Compos. Struct.*, 2023, **303**, 116136.

102 J. Zhou and J. P. Lucas, The effects of a water environment on anomalous absorption behavior in graphite/epoxy composites, *Compos. Sci. Technol.*, 1995, **53**(1), 57–64.

103 T. Zhang, Y. Xu, H. Li and B. Zhang, Interfacial adhesion between carbon fibers and nylon 6: Effect of fiber surface chemistry and grafting of nano-SiO₂, *Composites, Part A*, 2019, **121**, 157–168.

104 C. Bilgi, B. Demir, H. Aydın, B. Üstün and Ü. Kurtan, Effect of functionalized graphene nanoplatelet dispersion on thermal and electrical properties of hybrid carbon fiber reinforced aviation epoxy laminated composite, *Mater. Chem. Phys.*, 2024, **325**, 129702.

105 X. Yao, J. H. Hui, I. A. Kinloch and M. A. Bissett, Improved Mechanical Properties of Graphene/Carbon Fiber Composites via Silanization, *ACS Appl. Eng. Mater.*, 2024, **2**(7), 1836–1844.

106 *EMI Shielding Materials – Electrically Conductive Silicone*. **https://www.stockwell.com/emi-shielding-materials/**, (accessed June 8, 2025).

107 J. Chen, Y.-l Liu, D.-x Sun, X.-d Qi, J.-h Yang and Y. Wang, Recent progress in structural design of graphene/polymer porous composites toward electromagnetic interference shielding application, *Chem. Eng. J.*, 2024, **495**, 153586.

108 B. Ucpinar Durmaz, A. O. Salman and A. Aytac, Electromagnetic Interference Shielding Performances of Carbon-Fiber-Reinforced PA11/PLA Composites in the X-Band Frequency Range, *ACS Omega*, 2023, **8**(25), 22762–22773.

109 H. S. Ahmad, T. Hussain, Y. Nawab and H. Awais, Graphene and Fe₂O₃ filled composites for mitigation of electromagnetic pollution and protection of electronic appliances, *Compos. Sci. Technol.*, 2023, **240**, 110097.

110 X. Tan, Y. He, C. Wang, Y. Zhang, W. Wang, H. Li and R. Yu, Hierarchical mxene/Fe₃O₄/cellulose nanofiber composites with layer-by-layer architecture for high-performance electromagnetic interference shielding, *Compos. Sci. Technol.*, 2025, **265**, 111136.